

Impact of nanoscale magnetite and zero valent iron on the batch-wise anaerobic co-digestion of food waste and waste-activated sludge

Kassab, Ghada; Kather, Dima; Odeh, Fadwa; Shatanawi, Khaldoun ; Halalsheh, Maha; Arafah, Mazen ; van Lier, Jules B.

DOI

[10.3390/W12051283](https://doi.org/10.3390/W12051283)

Publication date

2020

Document Version

Final published version

Published in

Water (Switzerland)

Citation (APA)

Kassab, G., Kather, D., Odeh, F., Shatanawi, K., Halalsheh, M., Arafah, M., & van Lier, J. B. (2020). Impact of nanoscale magnetite and zero valent iron on the batch-wise anaerobic co-digestion of food waste and waste-activated sludge. *Water (Switzerland)*, 12(5), 1-19. Article 1283. <https://doi.org/10.3390/W12051283>

Important note

To cite this publication, please use the final published version (if applicable).
Please check the document version above.

Copyright




Other than for strictly personal use, it is not permitted to download, forward or distribute the text or part of it, without the consent of the author(s) and/or copyright holder(s), unless the work is under an open content license such as Creative Commons.

Takedown policy

Please contact us and provide details if you believe this document breaches copyrights.
We will remove access to the work immediately and investigate your claim.

Article

Impact of Nanoscale Magnetite and Zero Valent Iron on the Batch-Wise Anaerobic Co-Digestion of Food Waste and Waste-Activated Sludge

Ghada Kassab ^{1,*}, Dima Khater ², Fadwa Odeh ³ , Khaldoun Shatanawi ¹ , Maha Halalsheh ⁴, Mazen Arafah ⁵ and Jules B. van Lier ⁶ 

¹ Civil Engineering Department, School of Engineering, The University of Jordan, 11942 Amman, Jordan; kshatanawi@ju.edu.jo

² Department of Chemistry, Faculty of Art and Science, Applied Science Private University, 11931 Amman, Jordan; d_kahter@asu.edu.jo

³ Department of Chemistry, School of Science, The University of Jordan, 11942 Amman, Jordan; f.odeh@ju.edu.jo

⁴ Water, Energy and Environment Center, The University of Jordan, 11942 Amman, Jordan; halalshe@ju.edu.jo

⁵ Industrial Engineering Department, School of Engineering, The University of Jordan, 11942 Amman, Jordan; mazen.arafah@ju.edu.jo

⁶ Section Sanitary Engineering, Department of Water Management, Faculty of Civil Engineering and Geosciences, Delft University of Technology, 2628 CN Delft, The Netherlands; J.B.vanLier@tudelft.nl

* Correspondence: Ghada.kassab@ju.edu.jo; Tel.: +962-6-535-5000

Received: 29 February 2020; Accepted: 28 April 2020; Published: 30 April 2020



Abstract: As a potential approach for enhanced energy generation from anaerobic digestion, iron-based conductive nanoparticles have been proposed to enhance the methane production yield and rate. In this study, the impact of two different types of iron nanoparticles, namely the nano-zero-valent-iron particles (NZVIs) and magnetite (Fe₃O₄) nanoparticles (NPs) was investigated, using batch test under mesophilic conditions (35 °C). Magnetite NPs have been applied in doses of 25, 50 and 80 mg/L, corresponding to 13.1, 26.2 and 41.9 mg magnetite NPs/gTS of substrate, respectively. The results reveal that supplementing anaerobic batches with magnetite NPs at a dose of 25 mg/L induces an insignificant effect on hydrolysis and methane production. However, incubation with 50 and 80 mg/L magnetite NPs have instigated comparable positive impact with hydrolysis percentages reaching approximately 95% compared to 63% attained in control batches, in addition to a 50% enhancement in methane production yield. A biodegradability percentage of 94% was achieved with magnetite NP doses of 50 and 80 mg/L, compared to only 62.7% obtained with control incubation. NZVIs were applied in doses of 20, 40 and 60 mg/L, corresponding to 10.8, 21.5 and 32.2 mg NZVIs/gTS of substrate, respectively. The results have shown that supplementing anaerobic batches with NZVIs revealed insignificant impact, most probably due to the agglomeration of NZVI particles and consequently the reduction in available surface area, making the applied doses insufficient for measurable effect.

Keywords: anaerobic co-digestion; food wastes; waste-activated sludge; nano magnetite; iron oxide nano particles; nano zero valent iron; sewage sludge; nano particles; organic wastes

1. Introduction

Anaerobic digestion (AD) converts organic matter into biogas, a renewable source of energy, and digestate, a valuable fertilizer and soil conditioner [1,2]. Due to the increasing demand on renewable energy and the progressively adopted waste management policies that request diverting wastes from landfills, the AD process has been used for the treatment of different types of organic wastes, including

sewage sludge, food waste (FW), animal manure and agricultural wastes. Nevertheless, when FW is used as a single substrate, the digestion process stability can be hampered because of (i) a possible imbalance between acidogenesis and methanogenesis when high loads of rapid fermentable organic matter are applied, (ii) potential nutrients imbalance, a high carbon to nitrogen (C/N) ratio, and (iii) the high variability of FW composition [3]. A feasible and reliable approach to overcome these limitations is the use of sewage sludge as co-substrate for food waste digestion.

In the AD process, four major steps are involved, viz. hydrolysis, acidogenesis, acetogenesis and methanogenesis. Generally, the process is limited by one or two major steps, depending on the nature of the substrate. Hydrolysis is often the rate limiting step if complex organic solids are being digested. On the other hand, if the substrate is soluble organic matter, methanogenesis is generally the rate limiting step [4].

In recent years, several studies have shown that the supplementation of conductive nanoparticles has a positive effects on the anaerobic digestion process, particularly in relation to the enhancement of methane production yield and rate, the reduction in startup and recovery periods, in addition to stability improvement [5,6]. In particular, iron oxide nanoparticles (IONPs) that include magnetite, maghemite and hematite, in addition to the nano-zero-valent-iron particles (NZVIs) hold high potentials for AD enhancement and improvement of process robustness [5]. IONPs have specifically great potentials due to its high chemical stability and magnetic properties [7,8]. Most importantly, IONPs are conductive materials that may stimulate the direct interspecies electron transfer (DIET) in anaerobic digestion, in which interspecies electron transfer is not mediated by diffusive electron carriers (i.e. hydrogen or formate) but by direct transfer of electrons released from electron donating bacteria (i.e., oxidizing bacteria that can extracellularly release electrons to conductive materials) to electron capturing microorganism (i.e. methanogenic archaea) that can reduce carbon dioxide to methane using electrons transferred from the electron donating bacteria via the conductive materials [7,9]. The primary mechanism suggested to explain the enhancing behaviors of IONPs in syntrophic methanogenesis via DIET [10] is that (semi) conductive iron oxides act as electron conduits to accelerate DIET in syntrophic methanogenesis. Jiang et al. [11] suggested that electron transfer takes place via the biochemical dynamic cycling among the Fe(III) (mineral)-Fe (II)-Fe (III) mineral of the (semi)conductive iron oxides. Wherein, the released electrons are accepted by Fe(III) (mineral) of iron oxides and is reduced to produce Fe(II), then the unbounded Fe(II) transfers electron to methanogens. Fe(II) itself is readsorbed and oxidized back to original structural Fe(III) (mineral) through precipitation.

Early studies tackling the impact of IONPs on anaerobic digestion have used simple substrates (such as propionate, butyrate, and methanol), thus focusing on the syntrophic methanogenesis process. Kato et al. [12] showed that supplementing rice paddy soil with (semi)conductive iron oxide NPs (magnetite, hematite), significantly stimulated methanogenesis from acetate and ethanol in terms of onset time and production rate, attributing these results to the DIET through the (semi) conductive iron oxides. Possibly, in their research, syntrophic acetate oxidation was an important methanogenic pathway, although recent research showed a direct stimulatory effect of added hydrochar to the acetoclastic methanogen *Methanosaeta*, which was also ascribed to DIET [13]. Likewise, Zhang and Lu [14] showed that methane production from butyrate oxidation in lake sediments was significantly accelerated in the presence of magnetite NPs, suggesting that DIET mediated syntrophic methanogenesis. Focusing on methanogenic propionate degradation, Cruz Viggi et al. [15] showed that the supplementation of magnetite NPs to a methanogenic sludge obtained from a pilot scale anaerobic digester fed with wasted-activated sludge (WAS) resulted in a 33% enhancement in the maximum rate of methane production. Authors proposed that this stimulatory effect has most probably resulted from the establishment of a DIET with magnetite NPs serving as electron conduits between propionate oxidizing acetogens and carbon-dioxide-reducing methanogens.

The positive effects reported on the impact of conductive iron oxides on methane production yield and rate, using simple substrates, have pushed the research forward into studying the impact of IONPs on the anaerobic digestion of complex organics. Realizing that the hydrolysis of particulate organics is the rate limiting step in anaerobic digestion of complex organics, the majority of these

studies have investigated the impact of IONPs on the hydrolysis and acidification processes as well as on syntrophic methanogenesis [16–18]. The outcomes of these studies have shown that magnetite NPs can positively impact the hydrolysis of complex organic materials, thus providing abundant substrates for methanogens and promoting the anaerobic digestion process. Nevertheless, the mechanisms in which such impacts are attained are still not clear yet.

In a similar manner, several studies have been previously conducted to assess the impact of NZVIs on the anaerobic digestion process. Results have shown improvement on methane production yield with the supplementation of NZVIs, attributing such enhancement to:

- (i) The possibility of iron serving as an electron donor in the direct reduction of CO₂ to CH₄ by hydrogenotrophic methanogens [19–21];
- (ii) Shifting the fermentation pathway away from the propionic type because of the zero valent iron strong reducing property, which leads to the reduction in oxidation reduction potential (ORP) level [20,21];
- (iii) NZVIs serving as a conductive material to promote DIET [21].

Additionally, hydrogen evolution from iron corrosion could enhance both hydrogenotrophic methanogenesis and homoacetogenesis resulting from the increased H₂ flux as intermediary electron carrier [22–24], making the microbial consortia more susceptible for DIET. Other researchers observed that the addition of NZVIs leads to an increased conversion of complex organics to volatile fatty acids (VFAs) (i.e., improved hydrolysis and acidogenesis), which, in turn, enhanced the overall methanogenesis of complex substrates [25]. Yu et al. [26] studied the impact of NZVIs on the anaerobic digestion of WAS and found that the addition of 10 g/L NZVIs improved the hydrolysis-acidification process in which methanogenesis was completely inhibited. The results showed an 83% increase in total VFA concentration compared to the control incubation. The observed enhancement effect was accredited to enrichment of acid-forming bacteria, especially *Clostridia*. Feng et al. [22] also investigated the effect of NZVIs on the hydrolysis-acidification of waste-activated sludge when methanogenesis was inhibited. They observed an improvement in protein and polysaccharide conversion to 36.7% and 29.6%, respectively, at an NZVI dose of 4 g/L, compared to only 25.6% and 22.9% achieved in the control incubation. Moreover, the VFA production at an NZVI dose of 4 g/L was 37.3% higher compared to control incubation. Authors have attributed the enhanced hydrolysis-acidification to the increased activities of key enzymes. The results showed that the activities of protease and cellulase were increased by 85% at an NZVI dosage of 4 g/L, compared to the control incubations. The activities of acid-forming enzymes, including acetate kinase (AK), Phosphotransacetylase (PTA), butyrate kinase (BK) and phosphotransbutyrylase (PTB), were increased by 52.2% to 67.3%.

Despite the previously stated positive effects, NZVIs can cause inhibitory effects if added at elevated doses. Such inhibitory effects can be attributed to the strong reducing conditions developed at the NZVI surface, which can rapidly inactivate bacteria by causing severe damage to the cell membranes and to the respiratory activities through reductive decomposition of protein functional groups [27,28] and, possibly, to the rapid hydrogen production and accumulation that leads to the accumulation of VFAs [29].

Realizing the conceivable positive impacts of magnetite NPs and the NZVIs on the anaerobic digestion process, this research intended to study the effects of these two iron-based conductive materials on the co-digestion of food wastes and sewage sludge. This research aimed explicitly at investigating the impact of iron-based NPs on the hydrolysis process by measuring the extent of particulate organics solubilization. Moreover, the effects on the acidification and methane production yield and rate were examined as well.

2. Materials and Methods

2.1. Substrates and Inoculum

Two types of substrates were used in this study, FW and thickened WAS. FW was obtained from the main restaurant of the University of Jordan campus in Amman, Jordan; wherein, the entire

quantities of kitchen wastes and dishes leftovers produced in the sampling day (approximately 60 kg) were manually assorted to eliminate non-biodegradable materials, such as aluminum cans, glasses, styrofoam and plastic products. The residual food waste that included vegetables, fruits, dairy products, starchy food, and meat-based food was subsequently mixed thoroughly and approximately a 5-kg sample was collected. To ensure homogeneity and increase specific surface area, FW samples were subsequently grinded using a kitchen grinder and stored at 4 °C for less than two days before being used in the batch tests. It is worth mentioning that FW characterization was conducted using grinded samples. Thickened WAS was obtained from the Abu-Nussier Wastewater Treatment Plant (Amman, Jordan). The treatment plant receives a yearly average flow of 3700 m³/d of municipal wastewater with chemical oxygen demand (COD) and total suspended solids (TSS) concentrations of 960 and 470 mg/L, respectively.

Inoculum

Anaerobically digested sludge obtained from Al Shallaleh Wastewater Treatment Plant (Irbid, Jordan) was used as a source of inoculum. The anaerobic digester is a completely mixed reactor, operated at 37 °C and 20 days solids retention time. Total solids (TS) content of 21.2 g/L ± 1.4 was identified, along with volatile solids (VS) content of 15.2 g/L ± 0.85. The methanogenic activity test that was performed in triplicates using sodium acetate as the substrate at a concentration of 1 g/L and under initial substrate to inoculum ratio of 0.5gCOD/gVS [30] revealed an inoculum-specific methanogenic activity of 0.12 gCH₄-COD/gVS.d.

Before being used in the anaerobic digestion batch tests, the inoculum was pre-incubated under anaerobic conditions at 35 °C for four days to remove any residual biodegradable organic material that may have been present.

2.2. Preparation and Characteristics of the Nanoparticles

Magnetite NPs were synthesized according to the protocol described in Kang et al. [31]. A volume of 0.85 mL of 12.1 N HCl and 25 mL of purified deoxygenated water were combined and 5.2 g FeCl₃ along with 2.0 g FeCl₂ were dissolved into the solution under stirring conditions. The resulting solution was added drop wise into 250 mL of 1.5 M NaOH solution under vigorous stirring, generating an instant black precipitate of magnetite (Fe₃O₄). The precipitate was isolated using magnetic field (S-30-10 N webcraft Uster, Switzerland). Dynamic light scattering (DLS) data indicated a hydrodynamic size of 29.5 nm and polydispersity index of 0.91.

NZVI stock solution was freshly prepared by reducing ferrous chloride with sodium borohydride as reported by He et al. [32]. Briefly, 200 mL of 0.2 % w/w of sodium carboxy methyl cellulose (CMC, capping agent, Sigma –Aldrich) dissolved in deionized water was purged with high purity argon for at least 25 min. Then, 50 mL of 0.625 M of ferrous chloride tetrahydrate (FeCl₂·4H₂O, 98%, BBC chemicals) was gradually added to 200 mL of 0.2% CMC under argon gas purging. Finally, 31 mL of 4 M sodium borohydride (NaBH₄, 98%, Sigma Aldrich) was added drop wise to the 250 mL Fe-CMC complex while the solution was vigorously shaken at 1100 rpm at room temperature. The final concentrations of NZVIs and CMC in stock solution were 0.11 M and 0.14% w/w, respectively. DLS data indicated a hydrodynamic size of 110 nm and polydispersity index of 0.85.

2.3. Anaerobic Co-Digestion Batch Tests

Anaerobic batch tests were conducted using the OxiTop[®] system that is designed to collect and store pressure data. The tests were performed in triplicates using batch test bottles of 1000 mL (1135 mL working volume). Necessary macro and micronutrients were added according to Angelidaki et al. [33]. The substrate that consisted of FW and WAS was added at a ratio of 1.5:1 (FW: WAS), determined based on the VS content of each type of substrate. The amounts of substrate added were calculated according to Pabon et al. [34] and based on: (i) the maximum pressure increase allowed by the OxiTop measuring system, which is 0.3 atm, (ii) a minimum substrate concentration of 1 gCOD/L, (iii) a liquid

volume of 300 mL, and (iv) a maximum biomethane composition of 30%. As for the inoculum, the amounts added were based on a substrate to inoculum ratio of $1.0 \text{ gCOD}_{\text{substrate}}/\text{gVS}_{\text{inoculum}}$.

After the addition of medium solution, inoculum, substrate, and 200 mL of demineralized water, different aliquots of prepared nanoparticles stock solutions were added to reach desired nanoparticles concentrations. Afterward, demineralized water was added to reach 300 mL liquid volume and bottles were tightly sealed with OxiTop[®] measuring heads. Subsequently, the air in the headspace was flushed with nitrogen gas for 3 min to achieve anaerobic conditions. Then, bottles were incubated at $35 \pm 1 \text{ }^\circ\text{C}$ with continuous shaking at 100 rpm agitation speed. It is worth mentioning that the pressure that was built up in the first two hours was released since it is mainly due to the, dissolution of gases, upon temperature increase. For bottles used as the control, only the medium solution, inoculum, substrate that includes FW and WAS and demineralized water were added.

Biogas production was measured through the detection of pressure increase at constant volume, using the OxiTop[®] measuring heads. The methane content in the biogas was analyzed until the test was completed; i.e., the cumulative biogas curve reached a plateau. Soluble COD and VFA concentrations were followed by taking 2 mL of liquid sample every two days. Three blank bottles, containing all additions except substrates, were used to correct for inoculum methane production.

2.4. Analytical Methods

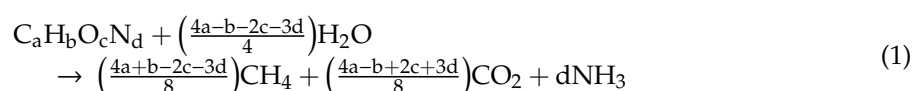
Total and volatile solids content were analyzed according to the Standard Methods for the Examination of Water and Wastewater [35]. Total nitrogen (TN), total phosphorous (TP), total ammonia nitrogen (TAN), chloride ion (Cl^-), in addition to the pH and electrical conductivity (EC) that were measured employing a waste to distilled water ratio of 1:10, were all analyzed according to Radojevic and Bashkin [36]. Elementary analyses of carbon, oxygen, hydrogen and nitrogen were performed using an elementary analyzer (Perkin-Elmer-Vector 8910) following the manufacturer's instructions.

To determine soluble COD and VFA for FW, a room temperature water extraction was performed on 25 g of grounded FW sample in 250 mL of distilled water for 1 h under agitation. The mixture was then centrifuged (3000 rpm) for 30 min and soluble COD and VFA were determined in the supernatant after being filtered using 0.45- μm filter paper. For WAS, the samples were immediately centrifuged and soluble COD and VFA were determined in the supernatant after filtration using 0.45- μm filter paper as well. Soluble COD was determined using the HACH Lange cuvette test and evaluated by a DR3900 HACH Lange Spectrophotometer. The individual VFAs (viz. acetic, propionic and butyric acids) were analyzed using a gas chromatograph (Varian 3300) equipped with packed column (2 m length, 2 mm internal diameter) and flame ionization detector (FID). Helium was used as the carrier gas at a flowrate of 30 mL/min. The detector temperature was 250 $^\circ\text{C}$. The pH of filtered sample was adjusted to less than 2 using formic acid prior to VFA analysis. Methane content in the biogas was analyzed using a gas chromatograph (PYE-NICAM 4500), equipped with packed column (1.5 m length, 4 mm internal diameter) and flame ionization detector (FID). Argon was used as a carrier gas at a flowrate of 30 mL/min. The detector temperature was 150 $^\circ\text{C}$. Certified gas standards (Spantech Products) were employed for the standardization of methane. Scanning electronic microscope (SEM) images were taken using the SEM Quanta Feg 450 instrument; samples were placed on carbon stub and sputtered with gold (5 mm thickness). As for the samples' insertion, image capturing and measurement were all performed according to manufacturer instruction.

3. Calculations

3.1. Theoretical Biochemical Methane Potential

The empirical mole composition of the FW and WAS, computed from the elementary analysis, allows for determining the theoretical biochemical methane potential (BMP_{Th}) relying on the stoichiometry of the substrate anaerobic degradation reaction [37].



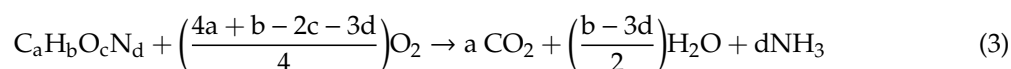
Therefore,

$$BMP_{Th} (LCH_4/kgVS) = \frac{22.4 \times ((4a + b - 2c - 3d)/8) \times 1000}{12a + b + 16c + 14d} \quad (2)$$

where 22.4 correspond to the volume (L) occupied by an ideal gas under standard conditions (temperature of 273 Kelvin (K) and pressure of 101.3 kpa). The 1000 refers to the volume conversion factor from L to mL.

3.2. Theoretical COD

The theoretical COD (COD_{Th}) can be computed from the stoichiometry of the substrate oxidation reaction



Therefore;

$$COD_{Th} (gCOD/gVS) = \frac{32 \times ((4a + b - 2c - 3d)/4)}{12a + b + 16c + 14d} \quad (4)$$

3.3. Experimental Biochemical Methane Potential

The experimental biochemical methane potential ($BMP_{experimental}$) was calculated based on the maximum methane production attained in batch test bottles after being corrected by the maximum methane production of the blank bottles [34].

$$\begin{aligned} & BMP_{experimental} (LCH_4/kgVS) \\ & = \frac{\left[\left(\frac{(P_s + P_{atm}) \times V}{R \times T}\right) \times CH_4\%_s\right] - \left[\left(\frac{(P_{blank} + P_{atm}) \times V}{R \times T}\right) \times CH_4\%_{blank}\right]}{S_o} \times 22.4 \end{aligned} \quad (5)$$

where P_s is the pressure accumulated inside the test bottle (pa), P_{atm} is the atmospheric pressure (pa), P_{blank} is the pressure accumulated in the blank bottle (pa), V is the headspace volume (m^3), T is the temperature in Kelvin (K), R is the universal gas constant, and $CH_4\%_s$ and $CH_4\%_{blank}$ are the accumulated biogas methane percent for the test and blank bottles, respectively. The S_o is the amount of substrate added in terms of VS.

3.4. Biodegradability, Hydrolysis and Acidification Percentages

Anaerobic biodegradability was assessed based on the percent of experimental BMP to the theoretical BMP.

$$Biodegradability\% = \frac{BMP_{experimental}}{BMP_{Th}} \times 100 \quad (6)$$

The hydrolysis percent was assessed based on the percent of the solubilized COD relative to the substrate initial particulate COD.

$$Hydrolysis\% = \frac{COD_{CH_4,t} + COD_{s,t} - COD_{s,t=0}}{COD_{Th,initial} - COD_{s,t=0}} \times 100 \quad (7)$$

where $COD_{CH_4,t}$ is the COD equivalent of methane produced at any time t , $COD_{s,t}$ is the soluble COD at any time t , $COD_{s,t=0}$ is the soluble COD at time $t = 0$ and $COD_{Th,initial}$ is the initial theoretical COD.

The acidification percent was assessed based on the percent of the acidified COD relative to the substrate initial theoretical COD.

$$\text{Acidification \%} = \frac{\text{COD}_{\text{CH}_4,t} + \text{COD}_{\text{VFA},t} - \text{COD}_{\text{VFA},t=0}}{\text{COD}_{\text{Th,initial}}} \times 100 \quad (8)$$

where $\text{COD}_{\text{CH}_4,t}$ is the COD equivalent of methane produced at any time t , $\text{COD}_{\text{VFA},t}$ is the VFA equivalent COD at any time t , $\text{COD}_{\text{VFA},t=0}$ is the VFA equivalent COD at time $t = 0$ and $\text{COD}_{\text{Th,initial}}$ is the initial theoretical COD.

3.5. Statistical Analysis

The statistical analyses were performed using the IBM SPSS statistics (version 23). Data collected for characterization of the FW and WAS were demonstrated with a mean (\bar{x}), standard deviation (σ) and coefficient of variation percent (CV). For the evaluation of the NZVIs and magnetite NPs' impact on the anaerobic co-digestion process, an ANOVA test with Bonferroni correction was used with a confidence interval of 95%.

3.6. Modeling of Methane Production

The modified Gompertz model was used to describe the progression of cumulative methane production [38].

$$Y(t) = Y_m \times \exp \left\{ - \exp \left[\frac{\mu_m \cdot e}{Y_m} \times (\lambda - t) + 1 \right] \right\} \quad (9)$$

where $Y(t)$ is the cumulative methane yield at a digestion time t (LCH_4/kgVS), Y_m is the maximum methane production (LCH_4/kgVS), μ_m is the maximum rate of methane production ($\text{LCH}_4/\text{kgVS}\cdot\text{d}$), λ is the lag phase time (d), and t is the incubation time (d), $e = \exp(1) = 2.718$.

4. Results and Discussions

4.1. Characteristics of Substrates

The average data and coefficient of variations for the FW and WAS characteristics are presented in Table 1. The FW-measured pH (4.1 ± 0.5) is indeed low compared to the average values reported in the literature. Fisgativa et al. [39], who compiled and analyzed FW characteristics data from 70 studies that evaluated 120 different food wastes, revealed an FW pH value of 5.1 ± 0.7 . Apparently, acidification was already instigated during storage time.

The total solid content of FW was 30%, which lies within the range stated in the literature, although it is among the highest reported [39–42]. The high VS/TS ratio (95.6%) highlights the high organic transformation potential. Nevertheless, the low level of soluble COD compared to theoretical COD (0.2) indicates the predominance of particulate COD in the FW, which can reduce the rate of degradation due to a limitation in hydrolysis.

The carbon to nitrogen ratio (C/N) of FW (17.6) is to some extent below the generally recommended level of 20–30 for an optimal anaerobic digestion process [40]. Moreover, upon co-digestion with the WAS that is generally characterized by a low C/N ratio (5.5), the resultant C/N ratio will be even lower. However, several researchers have demonstrated that the co-digestion of FW with WAS can be successfully performed under C/N ratios ranging from 8.8 to 13 [43–46].

With respect to nutrients content, the FW total Kjeldahl nitrogen (35.1 gN/kgVS) observed in this study is higher than the average values stated by Fisgativa et al. [39] but compatible to those reported by Zhang et al. [47], El Mashad and Zhang [48], Zhang et al. [49] and Agyeman and Tao [50] for types of FW similar to the one tested within this study. Phosphorous concentration (2.6 gP/kgVS) was found to be below the values reported in the literature [39,48,51], which are in the order of 5 gP/kgTS. Hence, in the context of nutrient supplementation, the comparison of the measured COD:N:P ratio (350:7.1:0.53), with what is reported in literature for successful and stable anaerobic digestion process (350:5:1) [52], confirms the deficiency of the phosphorous, for which the level obtained represents only 53% of the recommended value.

Table 1. Food waste (FW) and wasted-activated sludge (WAS) characteristics.

Parameter	n	FW		WAS	
		\bar{x} (σ)	CV (%)	\bar{x} (σ)	CV (%)
Physicochemical characteristics					
pH	8	4.1 (0.5)	12	7.4 (0.7)	10
TS (gTS/kg wet weight)	10	298.8 (21.6)	7		
(gTS/L)				25.2 (3.4)	13
VS (gVS/kg wet weight)	10	282.1 (24.6)	9		
(gVS/kgTS)		956.0 (10.9)	1		
(gVS/L)				21.1 (3.1)	15
Soluble COD (gO ₂ /kgVS)	8	311.2 (61.1)	20	654 (51)	8
(mg/L)					
Total Kjeldahl nitrogen (gN/kgVS)	8	35.1 (2.4)	7	107.7 (5.9)	5
Total ammonia nitrogen (gN/kg VS)	8	2.30 (0.5)	23	20 (3.0)	15
Total phosphorous (gP/kg VS)	8	2.6 (0.3)	13	20.9 (3.40)	16
Volatile fatty acids (g COD/kg VS)	8	3.7 (0.50)	12	13.10 (3.16)	24
C/N (%)		17.6		5.5	
Elementary analysis					
Carbon (%DM)	8	52.3 (4.7)	9	42.71 (3.14)	7
Hydrogen (%DM)	8	7.2 (0.8)	11	6.89 (0.6)	9
Oxygen (%DM)	8	37.1 (6.1)	16	42.5 (4.23)	10
Nitrogen (%DM)	8	3.4 (0.7)	20	7.9 (1.1)	14
Cl ⁻ (mg/kg DM)	8	11029 (1376.8)	12	6813 (991.6)	15

In regard of the ammoniacal nitrogen, the results obtained within this study (2.30 gN/kgVS) are considerably higher than those reported in the literature [39,53]. Increased ammonia concentrations result in an increased buffering capacity for the anaerobic digestion process.

On the whole, the FW and WAS mixture obtained physicochemical characteristics, which accentuate the numerous benefits of FW co-digestion with WAS: (i) improving the moisture content for wet digestion, taking into consideration the WAS moisture content of 97.8%, (ii) enhancing the nutrients balance for bacterial growth; total Kjeldahl nitrogen and total phosphorous contents in WAS equals of 107.7 gN/kgVS and 20.9 gP/kgVS, respectively, and (iii) the development of buffering capacity for the stable anaerobic digestion process.

In connection with the anaerobic biodegradability, the calculated BMP_{Th} for FW and WAS were 564.5 LCH₄/kgVS and 392.5 LCH₄/kgVS, respectively, computed based on the empirical mole composition of C_{18.0}H_{29.4}O_{9.6}N for FW and C_{6.3}H_{12.2}O_{4.7}N for WAS, assuming full COD conversion. The contribution of sulfur was considered negligible since the elementary analysis results, revealed below detection limit sulfur content. Also based on the empirical composition, the COD_{Th} for FW and WAS were 1.73 and 1.12 gO₂/gVS, respectively. It is worth mentioning that the COD_{Th} of the WAS deviated from the typical theoretical value of 1.42, which is linked to the overall elemental biomass composition C₅H₇O₂N. Apparently, the used WAS sample was more stabilized.

4.2. Effects of Magnetite NPs and NZVIs on Hydrolysis and Acidification

Due to the importance of hydrolysis in the kinetics of anaerobic digestion and the fact that it is usually the rate-limiting step, the impact of magnetite NPs on COD solubilization was assessed. Magnetite NP concentrations of 25, 50 and 80 mg/L were employed in anaerobic batch tests, corresponding to 13.1, 26.2 and 41.9 mg magnetite NPs/gTS of substrate calculated for the initial conditions. The results (Figure 1) show that the maximum soluble COD concentration achieved in the control incubation was 799 mg/L, which was reached after an incubation period of one day. Batches incubated with magnetite NPs had maximum soluble COD concentrations of 2280, 1852, and 1420 mg/L for magnetite NP doses of 80, 50 and 25 mg/L, respectively. Peak values were reached after six days with cumulative methane production of 49, 57 and 110 LCH₄/kgVS, for magnetite NP doses of 80, 50

and 25 mg/L, respectively. For the same incubation period (i.e., six days) the cumulative methane production in the control incubation reached 170 LCH₄/kgVS. Accordingly, to clarify whether increased soluble COD in magnetite NPs amended batches was due to the accumulation of soluble COD as a result of reduced consumption rates by methanogens (as discussed in Section 4.3 below) or due to stimulated hydrolysis, the hydrolysis percentages achieved after six days were computed. The results show that batches incubated with 80, 50 and 25 mg/L magnetite NPs, achieved hydrolysis percentages of 88%, 78%, and 55%, respectively, compared to hydrolysis percentage of 50% attained in control incubation. Hence, we concluded that magnetite NPs induced a stimulatory effect on the hydrolysis. The hydrolysis percentages achieved by the end of incubation periods in magnetite NPs amended batches were 65.1% for the 25 mg/L dose and 94.4% and 94.9% for the 50 and 80 mg/L doses, compared with 63.0% achieved in the control incubation. The positive impact induced by magnetite on hydrolysis process has been previously reported by several researchers. Zhao et al. [54], reported a twofold increase in waste-activated sludge protein hydrolysis, with magnetite (0.2 mm in diameter) dose of 10 g/L. Moreover, they have revealed an enhancement in the activity of protease and α -glycosidase enzymes by 63% and 27%, respectively. The positive impact of magnetite on hydrolysis of WAS was reported applying even bigger magnetite particle (8–12 mm), achieving a 31.2% and 11.6% increase in soluble protein and polysaccharides at a dose of 27 g/L [17]. Zhang et al. [18] reported that in batches incubated with 1 g/L magnetite NPs and with methanogenesis inhibition, the total polysaccharide decomposition was increased by 15.8% compared to the control incubation.

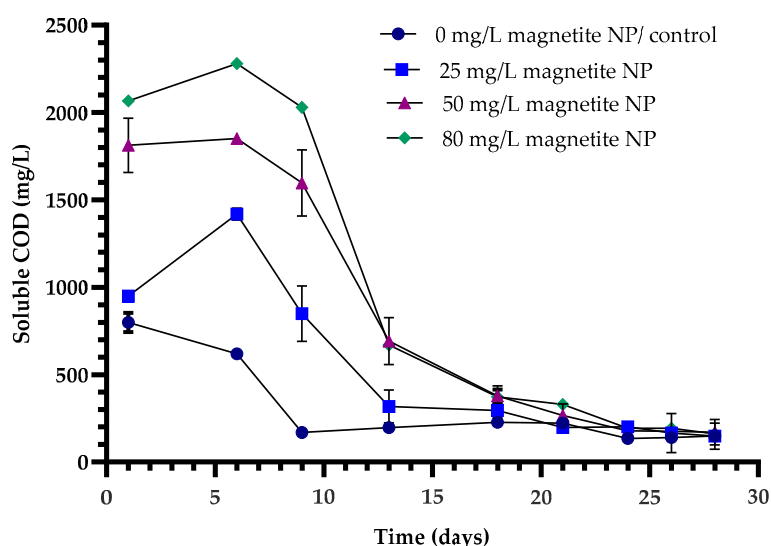


Figure 1. Effect of different magnetite NP doses on soluble COD.

Since methane yields are directly related to VFA production from substrate acidification, the impact of magnetite NPs on the availability of VFAs as precursors for methanogenesis was evaluated as well. The results show that acetate production was significantly stimulated, reaching maximum concentrations of 500, 749 and 1214 mg/L for magnetite NP doses of 25, 50 and 80 mg/L within 6 days, respectively, whereas the maximum acetate concentration in the control incubation was limited to 107 mg/L, which was reached after an incubation period of one day. Figure 2 shows that acetate was the predominant VFA, and its production is apparently directly related to the dose of the magnetite NPs. Concomitantly, methane production dropped with the increase in magnetite NPs. After the six-day incubation period, VFA concentrations started to decline, coinciding with the time at which the methane generation rate started to increase significantly, as shown in Section 4.3. To calculate the net increase in VFA production induced by magnetite NPs, the acidification percentage that takes into consideration methane production (i.e., VFA consumption) in addition to VFA generation, was computed after the six-day incubation period. The obtained results show a positive impact induced

by magnetite NPs on the acidification process, with percentages reaching 54.2%, 56.6%, and 84.0% in batches incubated with magnetite NPs doses of 25, 50, and 80 mg/L, respectively. This is compared to 40.0% achieved in the control incubation. These results are compatible with those reported by Zhao et al. [54], who also reported that acetate is the main VFA generated in magnetite-amended digesters, revealing a 1.6-fold increase in acetate concentration relative to the control when amino acids were used as the substrate, and a 1.75-fold increase over the control when monosaccharides were used as the substrate. Moreover, Zhang et al. [55], who assessed acidogenesis via hydrogen yield, revealed a 1.2-fold increase in hydrogen yield compared to the control upon addition of 50 mg/L magnetite NPs.

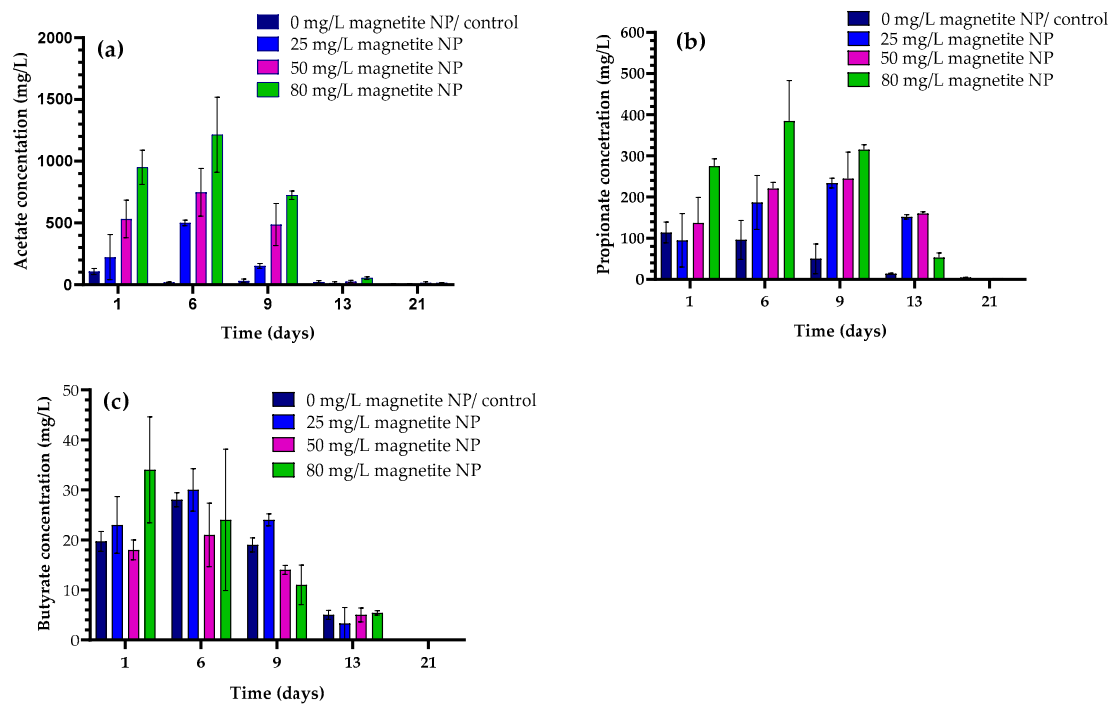


Figure 2. Effect of different magnetite NP doses on VFA production; (a) acetate, (b) propionate and (c) butyrate.

Magnetite NPs stimulatory impact on hydrolysis and acidification might be linked to the observed increased biomass aggregation that progressed along the incubation period, exclusively in batches incubated with magnetite NPs. Our results are congruent to the observed increased excretion of extracellular polymeric substances (EPS), brought about by magnetite supplementation, previously reported by Yin et al. [56] and Yan et al. [57]. Figure 3 shows formed aggregates after an incubation period of 8 days, along with the SEM images that were taken at the end of the incubation period. As shown by the SEM images, bacteria appeared to be aggregated and enveloped by what seems to be EPS, whereas the EPS fill the intercellular spaces within the aggregates. Observations support the hypothesis that enhanced EPS excretion may have played an essential adhesive role in the formation of aggregates and the maintenance of their integrity. Accordingly, considering the EPS sorptive capacities and their possible role in immobilizing the extracellular enzymes, the observed accelerated hydrolysis and acidification process can be explained by (i) the physical trapping of particulate and colloidal organics by means of the EPS, which leads to enhanced hydrolysis; (ii) immobilization and localization of extracellular enzymes by EPS; (iii) the minimization of hydrolysis and acidification product diffusion distances as a result of aggregation [58]. The enhanced aggregation of biomass and solid substrates implies that both enzymes and hydrolysis/acidification products remain relatively close to microbial cells, thus reducing the need for maintaining high levels of extracellular enzymes in the bulk solution and reducing the diffusive losses of products away from cells [59].

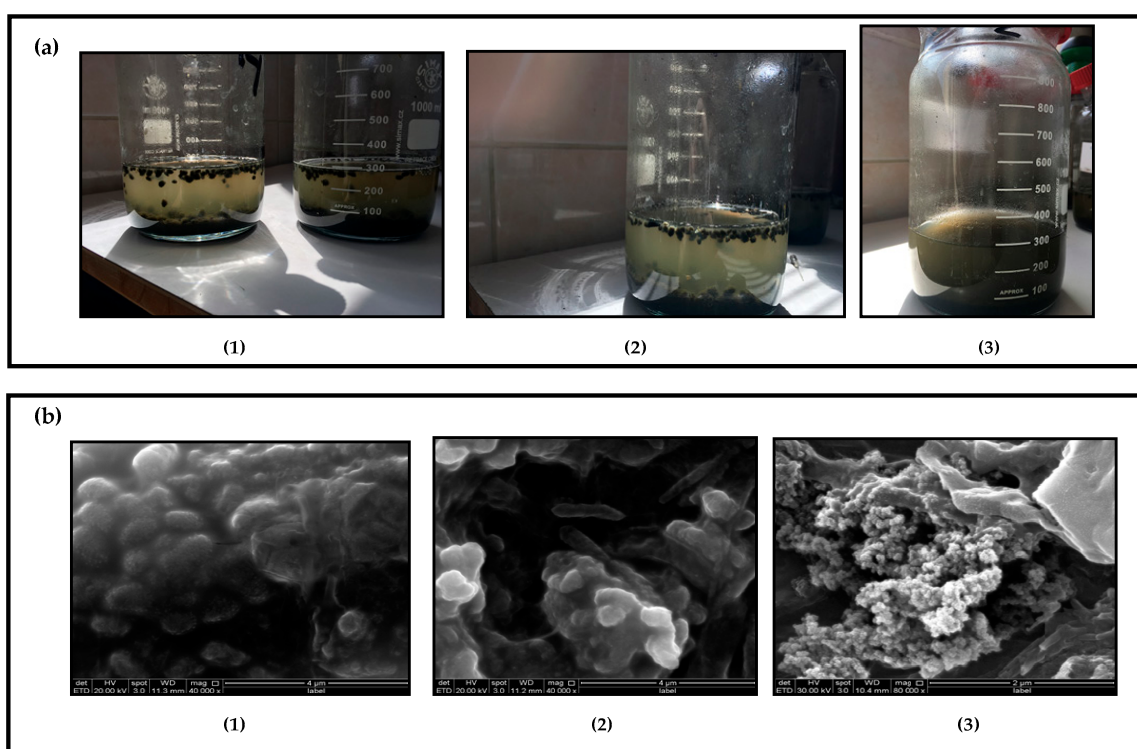


Figure 3. (a) Photos of the anaerobic batches, showing the biomass aggregation in batches incubated with magnetite NPs compared to the control incubation; (1) 80 mg/L (left) and 25 mg/L (right); (2) 50 mg/L, (3) 0 mg/L-control. (b) Scanning electronic microscope (SEM) images of aggregated biomass obtained from batches incubated with magnetite NPs by the end of the incubation period. (1) 25 mg/L; (2) 50 mg/L; (3) 80 mg/L.

Enhanced biomass aggregation resulting from magnetite nano or micro particles additions has been previously reported. Baek et al. [60,61] have studied the effect of magnetite particles (size 100–700 nm) supplementation on the anaerobic digestion of dairy effluent in a completely stirred tank reactor CSTR. Authors stated that added magnetite adhered to microbial cells' surfaces and induced microbial aggregation. Cruz Viggi et al. [15] and Li et al. [62] have studied the effect of magnetite particles on the anaerobic degradation of propionate and butyrate and showed through scanning electron microscopy analysis that the magnetite particles were adsorbed on cell surfaces. This resulted in larger agglomerates, with magnetite particles appeared bridging the microbial cells. Undoubtedly, the effect of IONPs on biomass aggregation needs to be explored further so as to help clarify possible functional mechanisms of these conductive materials in enhancing aggregation.

Concerning the impact of NZVIs, results showed only slight increases in soluble COD and VFA concentrations with increased doses of NZVIs along the whole incubation period (Figures 4 and 5). Nevertheless, calculated hydrolysis and acidification percentages showed a statistically insignificant difference. Possibly, the strong clustering or agglomeration of NZVIs particles caused this negligible effect.

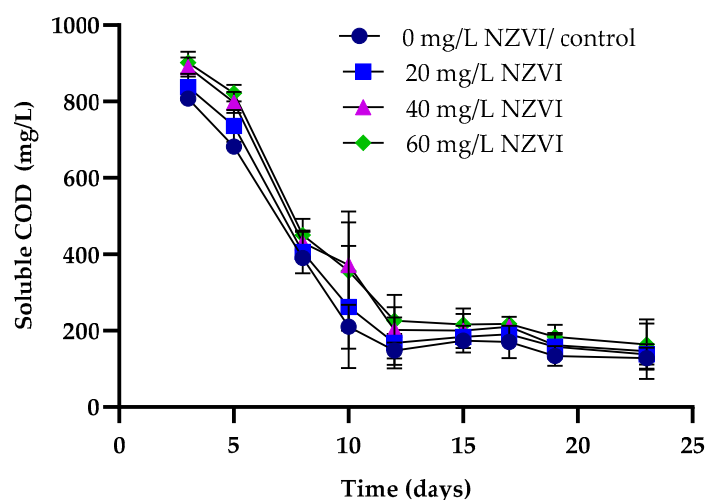


Figure 4. Effect of different nano-zero-valent-iron particle (NZVI) doses on soluble COD.

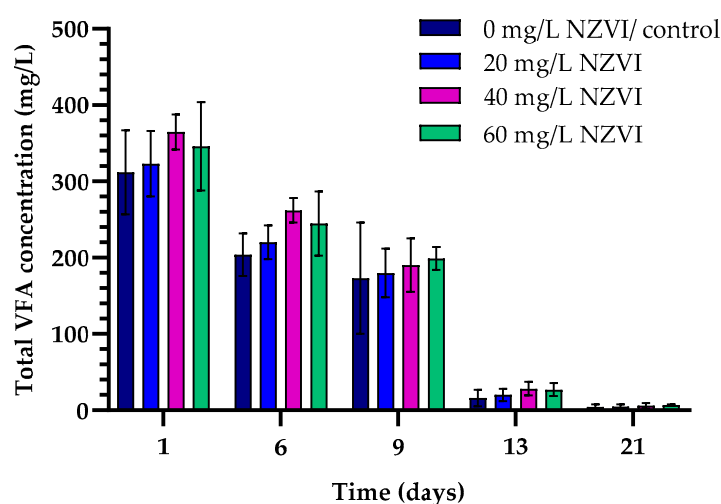


Figure 5. Effect of different nano-zero-valent-iron particle (NZVI) doses on total VFA production.

4.3. Effects of Magnetite NPs and NZVIs on Methane Production

The observed enhanced hydrolysis and acidification process will also impact subsequent methanogenesis. By the end of the incubation period, the cumulative methane production in the magnetite NPs amended batches (Section 4.3) reached 341.5, 478.3 and 481.5 LCH₄/kgVS, for magnetite NPs concentrations of 25, 50 and 80 mg/L, respectively. If compared with the control incubation, the batches incubated with magnetite NPs dose of 25 mg/L showed a methane production enhancement level of 7%, which was found to be statistically insignificant. With respect to the 50 and 80 mg/L magnetite NPs concentrations, results have shown a statistically significant increased methane production of 49.8% and 50.8%, respectively. These results resemble biodegradability percentages of 62.7% for the control incubation and 67.1%, 93.9% and 94.4% for incubations with 25, 50 and 80 mg/L magnetite NPs, respectively. Results undoubtedly indicated that addition of magnetite NPs increased methane production yield from anaerobic co-digestion of FW and WAS.

The addition of magnetite NPs to the batches, clearly retarded methanogenesis from the solubilized substrates (Figure 6), as also evidenced by the accumulating VFAs (Figure 2). Modeling experimental methane production data with the modified Gompertz model (Figure 6b) shows retardation periods (i.e. lag periods) of 2.8, 5.4 and 5.9 days for batches incubated with magnetite NPs doses of 25, 50, and 80 mg/L, respectively. However, after this period, the maximum methane production rate was accelerated, especially for batches incubated with magnetite NPs doses of 50 and 80 mg/L to attain an

increase of 21.3% and 45.2%, relative to the control incubation (Figure 7). The initial retardation might be due to the rapid acid production resulting in a low local pH, initially inhibiting methanogenesis. Further research is required to unravel the observed phenomenon. However, if compared with the control incubation, the enhanced methane production yield in magnetite amended batches can be undoubtedly attributed to improved hydrolysis and acidification.

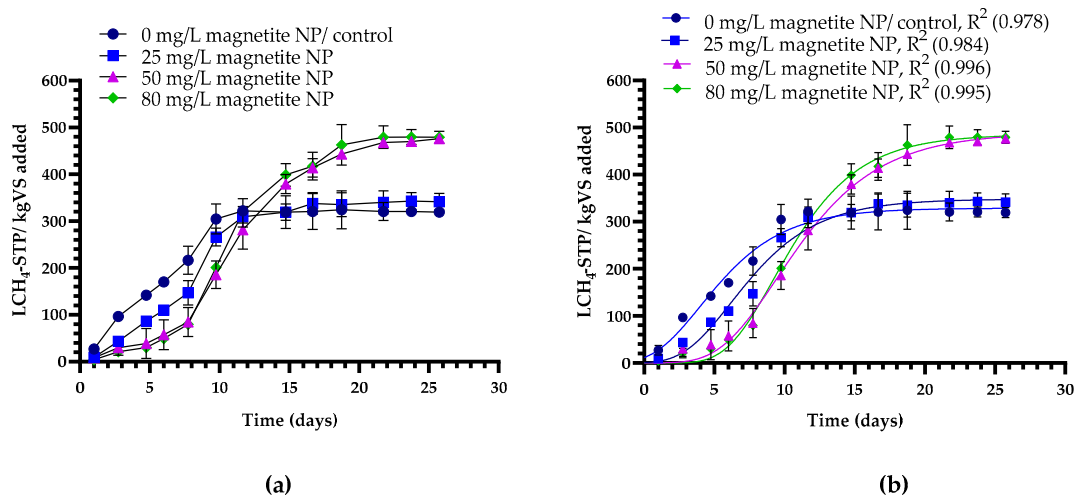


Figure 6. Cumulative methane production at different magnetite NP doses; (a) experimental data, (b) modified Gompertz model fit.

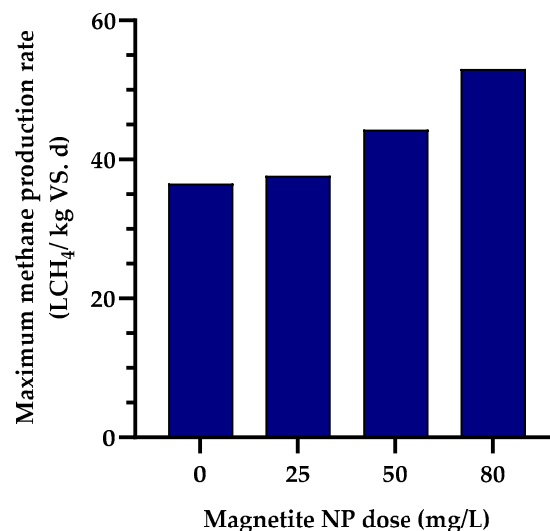


Figure 7. Effect of different magnetite NP doses on maximum methane production rates, computed from the modified Gompertz model.

Concerning the impact of NZVIs (Figure 8), the statistical analysis of computed results has revealed no measurable effect on methane generation for the three applied doses of 20, 40, and 60 mg NZVIs/L, which are equivalent to 10.8, 21.5 and 32.2 mg NZVIs/gTS of substrate, respectively. In details, the cumulative methane production at NZVIs doses of 20, 40 and 60 mg/L were 332.4, 338.3 and 343.0 LCH₄/kgVS, compared to 341.6 LCH₄/kgVS obtained with the control incubation. In literature, the impact of NZVIs on anaerobic digestion has been assessed either related to toxicity phenomena or conversion rate enhancement. The studies focusing on toxicity assessment have employed doses in the range of 55–2000 mg/L of NZVIs. Yang et al. [29] studied the impact of NZVIs on flocculent anaerobic sludge using glucose as the substrate and reported methane production inhibition levels of 20% at NZVIs doses of 1 and 10 mM (i.e. 55.9 and 558.5 mg NZVIs/L). Elevating the NZVIs dose

to 30 mM (1675.5 mg NZVIs/L) resulted in 69% methane production inhibition. Authors attributed the increased inhibition to increased hydrogen accumulation resulting in reduced VFA conversion. He et al. [63] have also reported substantial methane production inhibition at NZVIs doses of 30 mM (1675.5 mg NZVIs/L) applied to flocculent sewage sludge. Jia et al. [64] have reported not only methane production inhibition but also a lag period of 15 days when treating flocculent sewage sludge with NZVIs doses of 1500 and 2000 mg/L. Studies focusing on methane production enhancement have employed NZVIs doses in the range of 1 to 10 mg NZVIs/gTS, with greater attention given to the impact on anaerobic digestion of sewage sludge. Su et al. [19] and Suanon et al. [65] have shown that the anaerobic digestion of sewage sludge in the presence of NZVIs at a concentration of 1 and 5 mg NZVIs/gTS resulted in 40.4% and 45.8% methane production yield enhancement. Substantially higher enhancement levels were achieved by Lizama et al. [21] at NZVIs doses of 3.4, 4.7 and 6.0 mg NZVIs/gTS, attaining enhancement levels of 88%, 126%, and 186%, respectively. Putting the results of this study in the context of previous studies shows that with the applied doses of the NZVIs, an enhancement of methane production is anticipated. It is considered that the insignificant impact attained may be attributed to the aggregation of NZVIs particles in form of clusters. Expectedly, aggregation of NZVIs particles will adversely affect their activity since increased size will inevitably reduce the hydrogen and ferrous iron release rates [29,66]. Consequently, the doses employed in this study may have become insufficient to lead into a notable enhancement in methane production. Actually, several previous studies have accentuated on NZVIs strong tendency for aggregation, particularly due to attractive magnetic interaction [29,67,68]. Accordingly, further investigations on the impact of NZVIs on anaerobic digestion are certainly indispensable.

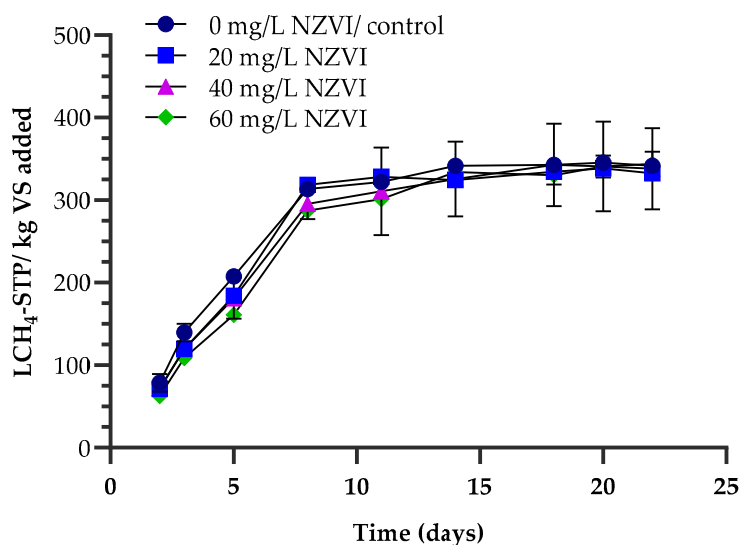


Figure 8. Cumulative methane production at different nano-zero-valent-iron particle (NZVI) doses.

5. Economic and Environmental Considerations

The obtained results, with the significant increase in methane production yield, show that supplementing the co-digestion process with magnetite NPs presents an opportunity for increased economic feasibility. On the one hand, improved methane production efficiency implies increased revenues from the elevated generation of power and heat energy. Moreover, the fact that magnetite NPs are inexpensive to produce [69,70] and can be effectively separated and reused [71] will only limitedly increase the operational costs. On the other hand, realizing effective industrial implementation necessitates a detailed economic analysis that requires further technical and scientific research to specify critical technical information, such as the maximum endurable organic loading rates, and optimum magnetite NP dose, both determined according to substrate characteristics and operating conditions.

Moreover, the results show that the addition of magnetite NPs, enhances anaerobic biodegradability percentages substantially, which consequently leads to higher volatile solids destruction. Accordingly, the quantities of generated digestate will be reduced, and thus the capital and operational cost of post digestion processes will be decreased. However, the impact of using magnetite NPs on the quality of the digestate needs to be investigated in conjunction with different operating conditions and magnetite NP doses. Particularly, if generated digestate is being considered for use as organic fertilizers. On the positive side, numerous studies have shown that IONPs have a beneficial impact on plants and lead to the improvement of crop agronomic traits [72–77]. Other studies, with the purpose of discarding toxic impacts, have shown that irrigating with water solutions containing magnetite NP concentrations as high as 1000 mg/L [78] or foliar feeding with magnetite NP solution of 10,000 mg/L [79], had no toxic impacts on plant growth. Nevertheless, and despite such promising results, the effects associated with the presence of magnetite NPs in digestate vary according to the physical and chemical characteristics of nanoparticles, soil characteristics, plant species, in addition to the rate of applications. Thus, the use of magnetite NPs on industrial scale necessitates integrated planning and management that must be supported by scientific customized studies.

6. Conclusions

This study investigated the effect of magnetite nanoparticles and nano-zero-valent-iron particles on the anaerobic co-digestion of food waste with sewage sludge. The results show that supplementing anaerobic co-digestion batches with magnetite NPs at doses of 26.2 and 41.9 mg magnetite NPs/gTS has led to a significant increase in hydrolysis percentages to a level of 94.4% and 94.8%, respectively. This is compared to 63.0% attained with the control incubation. Acidification was significantly improved as well, with acetate being the predominant VFA. Acidification percentages reached 56.6% and 84.0% in batches incubated with magnetite NP doses of 26.2 and 41.9 mg magnetite NPs/gTS, respectively, compared to only 40.0% achieved in the control incubation. The cumulative methane production yield reached 478.3 and 481.5 LCH₄/kgVS in batches incubated with 26.2 and 41.9 mg magnetite NPs/gTS, respectively. These production yields present an increase of 49.8% and 50.8% compared to the yield attained in the control incubation. Regarding the effect of nano-zero-valent-iron particles, the results show no impact, neither on methane production nor on hydrolysis or acidification.

Author Contributions: Conceptualization, G.K., F.O. and M.H.; Data curation, K.S. and M.A.; Formal analysis, J.B.v.L.; Funding acquisition, G.K.; Investigation, G.K., D.K. and F.O.; Methodology, G.K. and D.K.; Project administration, G.K.; Writing—original draft, G.K.; Writing—review & editing, M.H. and J.B.v.L. All authors have read and agreed to the published version of the manuscript.

Funding: This research was funded by Abdul Hameed Shoman Foundation/ The Scientific Research Support Fund (3/2016). Jordan.

Conflicts of Interest: The authors declare no conflict of interest

References

1. Lacovidou, E.; Ohandja, D.; Voulvoulis, N. Food waste co-digestion with sewage sludge-Realizing potential in the UK. *J. Environ. Manag.* **2012**, *112*, 267–274. [[CrossRef](#)]
2. Mehariya, S.; Patel, A.; Obulisamy, P.; Punniyakotti, E. Co-digestion of food waste and sewage sludge for methane production: Current status and perspectives. *Bioresour. Technol.* **2018**, *265*, 519–531. [[CrossRef](#)]
3. Kim, M.; Chowdhury, M.; Nakhla, G.; Keleman, M. Synergism of co-digestion of food wastes with municipal wastewater treatment biosolids. *Waste Manag.* **2017**, *61*, 473–483. [[CrossRef](#)] [[PubMed](#)]
4. Ma, J.; Frear, C.; Wang, Z.; Yu, L.; Zhao, Q.; Li, X.; Chen, S. A simple methodology for rate limiting step determination for anaerobic digestion of complex substrates and effect of microbial community ratio. *Bioresour. Technol.* **2013**, *134*, 391–395. [[CrossRef](#)] [[PubMed](#)]
5. Yang, Y.; Zhang, C.; Hu, Z. Impact of metallic and metal oxide nanoparticles on wastewater treatment and anaerobic digestion. *Environ. Sci. Process Impacts* **2013**, *15*, 39–48. [[CrossRef](#)] [[PubMed](#)]

6. Lee, Y.; Lee, D. Impact of adding metal nanoparticles on anaerobic digestion performance-A review. *Bioresour. Technol.* **2019**, *121926*, 1–9. [[CrossRef](#)]
7. Park, J.; Kang, H.; Park, K.; Park, H. Direct interspecies electron transfer via conductive materials: A perspective for anaerobic digestion applications. *Bioresour. Technol.* **2018**, *254*, 300–311. [[CrossRef](#)]
8. Sekoai, P.; Ouma, C.; du Preez, S.; Modisha, P.; Engelbrecht, N.; Bessarabov, D.; Ghimire, A. Application of nanoparticles in biofuels: An overview. *Fuel* **2019**, *237*, 380–397. [[CrossRef](#)]
9. Baek, G.; Kim, J.; Kim, J.; Lee, C. Role and potential of direct interspecies electron transfer in anaerobic digestion. *Energies* **2018**, *11*, 107. [[CrossRef](#)]
10. Xu, H.; Chang, J.; Wang, H.; Liu, Y.; Zhang, X.; Liang, P.; Huang, X. Enhancing direct interspecies electron transfer in syntrophic methanogenic association with semi conductive iron oxides: Effects and mechanisms. *Sci. Total Environ.* **2019**, *695*, 133876. [[CrossRef](#)]
11. Jiang, S.; Park, S.; Yoon, Y.; Lee, J.; Wu, W.; Phuoc Dan, N. Methanogenesis facilitated by geo-biochemical iron cycle in a novel syntrophic methanogenic microbial community. *Environ. Sci. Technol.* **2013**, *47*, 10078–10084. [[CrossRef](#)] [[PubMed](#)]
12. Kato, S.; Hashimoto, K.; Watanabe, K. Methanogenesis facilitated by electric syntrophy via (semi)conductive iron oxide minerals. *Environ. Microbiol.* **2012**, *14*, 1646–1654. [[CrossRef](#)] [[PubMed](#)]
13. Ren, S.; Usman, M.; Tsang, D.; O'thong, S.; Angelidaki, I.; Zhu, X.; Zhang, S.; Luo, G. Hydrochar-facilitated anaerobic digestion: Evidence for direct interspecies electron transfer mediated through surface oxygen-containing functional groups. *Environ. Sci. Technol.* In press.
14. Zhang, J.; Lu, Y. Conductive Fe₃O₄ nanoparticles accelerate syntrophic methane production from butyrate oxidation in two different lake sediments. *Front. Microbiol.* **2016**, *7*, 1316–1325. [[CrossRef](#)]
15. Cruz Viggì, C.; Rossetti, S.; Fazi, S.; Paiano, P.; Majone, M. Magnetite particles triggering a faster and more robust syntrophic pathway of methanogenic propionate degradation. *Environ. Sci. Technol.* **2014**, *48*, 7536–7543. [[CrossRef](#)]
16. Zhao, Z.; Zhang, Y.; Li, Y.; Quan, X.; Zhao, Z. Comparing the mechanisms of ZVI and Fe₃O₄ for promoting waste activated sludge digestion. *Water Res.* **2018**, *1444*, 126–133. [[CrossRef](#)]
17. Pong, H.; Zhang, Y.; Tan, D.; Zhao, Z.; Zhao, H.; Quan, X. Roles of magnetite and granular activated carbon in improvement of anaerobic sludge digestion. *Bioresour. Technol.* **2018**, *249*, 666–672. [[CrossRef](#)]
18. Zhang, Y.; Zhaohui, Y.; Xu, R.; Xiang, Y.; Jia, M.; Hu, J.; Zheng, Y.; Xiong, W.; Cao, J. Enhanced mesophilic anaerobic digestion of waste sludge with the iron nanoparticles addition and kinetic analysis. *Sci. Total Environ.* **2019**, *686*, 124–133. [[CrossRef](#)]
19. Su, L.; Shi, X.; Gun, G.; Zhano, A.; Zhao, Y. Stabilization of sewage sludge in the presence of nanoscale zero valent iron (nZVI): Abatement of odor and improvement of biogas production. *J. Mater. Cycles Waste* **2013**, *15*, 461–468. [[CrossRef](#)]
20. Abdelsalam, E.; Samer, M.; Attia, Y.; Abdel Hadi, M.; Hassan, H.; Badr, Y. Influence of zero valent iron nanoparticles and magnetic iron oxide nanoparticles on biogas and methane production from anaerobic digestion of manure. *Energy* **2017**, *120*, 842–853. [[CrossRef](#)]
21. Lizama, A.; Figueiras, C.; Pedreguera, A.; Espinoza, J. Enhancing the performance and stability of the anaerobic digestion of sewage sludge by zero valent iron nanoparticles dosage. *Bioresour. Technol.* **2019**, *275*, 352–359. [[CrossRef](#)] [[PubMed](#)]
22. Feng, Y.; Zhang, Y.; Quan, X.; Chen, S. Enhanced anaerobic digestion of waste activated sludge digestion by the addition of zero valent iron. *Water Res.* **2014**, *52*, 242–250. [[CrossRef](#)] [[PubMed](#)]
23. Hao, X.; Wei, J.; van Loosdrecht, M.; Cao, D. Analyzing the mechanisms of sludge digestion enhanced by iron. *Water Res.* **2017**, *117*, 58–67. [[CrossRef](#)] [[PubMed](#)]
24. Baek, G.; Kim, J.; Lee, C. A review of the effects of iron compounds on methanogenesis in anaerobic environments. *Renew. Sust. Energy Rev.* **2019**, *113*, 109282. [[CrossRef](#)]
25. Wei, W.; Cai, Z.; Fu, J.; Xie, G.; Li, A.; Zhou, X.; Ni, B. Zero valent iron enhances methane production from primary sludge in anaerobic digestion. *Chem. Eng. J.* **2018**, *351*, 1159–1165. [[CrossRef](#)]
26. Yu, B.; Huang, X.; Zhang, D.; Lou, Z.; Yuan, H.; Zhu, N. Response of sludge fermentation liquid and microbial community to nano zero valent iron exposure in a mesophilic anaerobic digestion system. *RSC Adv.* **2016**, *6*, 24236–24243. [[CrossRef](#)]
27. Lee, C.; Kim, J.; Lee, W.; Nelson, K.; Yoon, J.; Sedlak, D. Bactericidal effect of zero valent iron nanoparticles on *Escherichia coli*. *Environ. Sci. Technol.* **2008**, *42*, 4927–4933. [[CrossRef](#)]

28. Kim, J.; Park, H.; Lee, C.; Kara, N.; Sedlak, D.; Yoon, J. Inactivation of *Escherichia coli* by nano particulate zero valent iron and ferrous ion. *Appl. Environ. Microbiol.* **2010**, *76*, 7668–7670. [[CrossRef](#)]
29. Yang, Y.; Guo, J.; Hu, Z. Impact of nano zero valent iron (NZVI) on methanogenic activity and population dynamics in anaerobic digestion. *Water Res.* **2013**, *47*, 6790–6800. [[CrossRef](#)]
30. Cho, Y.; Young, J.; Jordan, J.; Moon, H. Factors affecting measurement of specific methanogenic activity. *Water Sci. Technol.* **2005**, *52*, 435–440. [[CrossRef](#)]
31. Kang, Y.; Risbud, S.; Rabolt, J.; Stroeve, P. Synthesis and characterization of nanometer size Fe₃O₄ and Fe₂O₃ particles. *Chem. Mater.* **1996**, *8*, 2209–2211. [[CrossRef](#)]
32. He, F.; Zhao, D.; Liu, J.; Roberts, C. Stabilization of Fe-Pd nanoparticles with sodium carboxymethyl cellulose for enhanced transport and dechlorination of trichloroethylene in soil and groundwater. *Ind. Eng. Chem. Res.* **2007**, *46*, 29–34. [[CrossRef](#)]
33. Angelidaki, I.; Alves, M.; Bolzonella, D.; Borzacconi, L.; Campos, J.; Guwy, A.; Kalyuzhnyi, S.; Jenicke, P.; van Lier, J. Defining the biomethane potential (BMP) of solid organic wastes and energy crops: A proposed protocol for batch assays. *Water Sci. Technol.* **2009**, *59*, 927–934. [[CrossRef](#)] [[PubMed](#)]
34. Pabon, P.; Castanares, G.; van Lier, J. An oxiTop protocol for screening plant material for its biochemical methane potential (BMP). *Water Sci. Technol.* **2012**, *66*, 1416–1423. [[CrossRef](#)] [[PubMed](#)]
35. Baird, R.; Bridgewater, L. *Standard Methods for the Examination of Water and Wastewater*, 23rd ed.; American Public Health Association: Washington, DC, USA, 2017.
36. Radojevic, M.; Bashkin, V. *Practical Environmental Analysis*; RSC Publishing: Cambridge, UK, 2006.
37. Buswell, A.; Mueller, H. Mechanism of methane fermentation. *Ind. Eng. Chem.* **1952**, *44*, 550–552. [[CrossRef](#)]
38. Elbeshbishy, E.; Nakhla, G. Batch anaerobic co-digestion of proteins and carbohydrates. *Bioresour. Technol.* **2012**, *116*, 170–178. [[CrossRef](#)]
39. Fisgativa, H.; Tremier, A.; Dabert, P. Characterizing the variability of food waste quality: A need for efficient valorization through anaerobic digestion. *Waste Manag.* **2016**, *50*, 264–274. [[CrossRef](#)]
40. Zhang, C.; Su, H.; Baeyens, J.; Tan, T. Reviewing the anaerobic digestion of food waste for biogas production. *Renew. Sust. Energy Rev.* **2014**, *38*, 383–392. [[CrossRef](#)]
41. Liu, C.; Li, H.; Zhang, Y.; Liu, C. Improve biogas production from low-organic- content sludge through high-solids anaerobic co-digestion with food waste. *Bioresour. Technol.* **2016**, *219*, 252–260. [[CrossRef](#)]
42. Fisgativa, H.; Tremier, A.; Roux, S.; Bureau, C.; Dabert, P. Understanding the anaerobic biodegradability of food waste: Relationship between the typological, biochemical and microbial characteristics. *J. Environ. Manag.* **2017**, *188*, 95–107. [[CrossRef](#)]
43. Liu, L.; He, Q.; Ma, Y.; Wang, X.; Peng, X. A mesophilic anaerobic digester for treating food waste: Process stability and microbial community analysis using pyro sequencing. *Microb. Cell Factories* **2016**, *15*, 1–11. [[CrossRef](#)] [[PubMed](#)]
44. Dai, X.; Duan, N.; Dong, B.; Dai, L. High solids anaerobic co-digestion of sewage and food waste in comparison with mono digestion: Stability and performance. *Waste Manag.* **2013**, *33*, 308–316. [[CrossRef](#)] [[PubMed](#)]
45. Gou, C.; Yang, Z.; Huang, J.; Wang, H.; Xu, H.; Wang, L. Effects of temperature and organic loading rate on the performance and microbial community of anaerobic co-digestion of waste activated sludge and food waste. *Chemosphere* **2014**, *105*, 146–151. [[CrossRef](#)] [[PubMed](#)]
46. Koch, K.; Plabst, M.; Schmidt, A.; Helmreich, B.; Drewes, J. Co-digestion of food waste in a municipal wastewater treatment plant: Comparison of batch tests and full scale experiences. *Waste Manag.* **2016**, *47*, 28–33. [[CrossRef](#)]
47. Zhang, R.; El-Mashad, H.; Hartman, K.; Wang, F.; Liu, G.; Choate, C.; Gamble, P. Characterization of food waste as feedstock for anaerobic digestion. *Bioresour. Technol.* **2007**, *98*, 929–935. [[CrossRef](#)]
48. El-Mashad, H.; Zhang, R. Biogas production from co-digestion of dairy manure and food waste. *Bioresour. Technol.* **2010**, *101*, 4021–4028. [[CrossRef](#)]
49. Zhang, L.; Lee, Y.; Jahng, D. Anaerobic co-digestion of food waste and piggery wastewater: Focusing on the role of trace elements. *Bioresour. Technol.* **2011**, *102*, 5048–5059. [[CrossRef](#)]
50. Agyeman, F.; Tao, W. Anaerobic co-digestion of food waste and dairy manure: Effects of food waste particle size and organic loading rate. *J. Environ. Manag.* **2014**, *133*, 268–274. [[CrossRef](#)]
51. Zhang, Y.; Banks, C.; Heaven, S. Co-digestion of source segregated domestic food waste to improve process stability. *Bioresour. Technol.* **2012**, *114*, 168–178. [[CrossRef](#)]

52. Von Sperling, M.; Chernicharo, C. *Biological Wastewater Treatment in Warm Climate Regions*; IWA Publishing: London, UK, 2005.
53. El-Mashad, H.; Zhang, R. Co-digestion of food waste and dairy maure for biogas production. *Tasabe* **2007**, *50*, 1815–1821.
54. Zhao, Z.; Li, Y.; Yu, Q.; Zhang, Y. Ferroferric oxide triggered possible direct interspecies electron transfer between syntrophomonas and Methanosaeta to enhance waste activated sludge anaerobic digestion. *Bioresour. Technol.* **2018**, *250*, 79–85. [[CrossRef](#)] [[PubMed](#)]
55. Zhang, Z.; Guo, L.; Wang, Y.; Zhao, Y.; She, Z.; Gao, M.; Guo, Y. Application of iron oxide (Fe₃O₄) nanoparticles during the two stage anaerobic digestion with waste sludge: Impact on the biogas production and the substrate metabolism. *Renew. Energy* **2020**, *146*, 2724–2735. [[CrossRef](#)]
56. Yin, Q.; He, K.; Echigo, S.; Wu, G.; Zhan, X.; Hu, H. Ferroferric oxide significantly affected production soluble microbial products and extracellular polymeric substances in anaerobic methangogenesis reactors. *Front. Microbiol.* **2018**, *9*, 2376. [[CrossRef](#)] [[PubMed](#)]
57. Yan, W.; Sun, F.; Liu, J.; Zhao, X. Enhanced anaerobic phenol degradation by conductive materials via EPS and microbial community alteration. *Chem. Eng. J.* **2018**, *352*, 1–9. [[CrossRef](#)]
58. Oh, S.; Kang, S.; Azizi, A. Electrochemical communication in anaerobic digestion. *Chem. Eng. J.* **2018**, *353*, 878–889. [[CrossRef](#)]
59. Hoffman, M.; Decho, A. Extracellular enzymes within microbial biofilms and the role of the extracellular polymer matrix. In *Microbial Extracellular Polymeric Substances: Characterization, Structure and Function*, 1st ed.; Wingender, J., Neu, T., Flemming, H., Eds.; Springer: Berlin/Heidelberg, Germany, 1999; pp. 217–227.
60. Baek, G.; Kim, J.; Lee, C. A long study on the effect of magnetite supplementation in continuous anaerobic digestion of dairy effluent-Enhancement in process performance and stability. *Bioresour. Technol.* **2016**, *222*, 344–354. [[CrossRef](#)]
61. Baek, G.; Jung, H.; Kim, J.; Lee, C. A long-term study on the effect of magnetite supplementation in continuous anaerobic digestion of dairy effluent. *Bioresour. Technol.* **2017**, *241*, 830–840. [[CrossRef](#)]
62. Li, H.; Chang, J.; Liu, P.; Fu, L.; Ding, D.; Lu, Y. Direct interspecies electron transfer accelerates syntrophic oxidation of butyrate in paddy soil enrichments. *Environ. Microbiol.* **2014**, *17*, 1533–1547. [[CrossRef](#)]
63. He, C.; He, P.; Yang, H.; Li, L.; Lin, Y.; Mu, Y. Impact of zero-valent iron nanoparticles on the activity of anaerobic granular sludge: From macroscopic to microcosmic investigation. *Water Res.* **2017**, *127*, 32–40. [[CrossRef](#)]
64. Jia, T.; Wang, Z.; Shan, H.; Liu, Y.; Lei, G. Effect of nanoscale zero-valent iron on sludge anaerobic digestion. *Resour. Conserv. Recycl.* **2017**, *127*, 190–195. [[CrossRef](#)]
65. Suanon, F.; Sun, Q.; Mama, D.; Li, J.; Dimon, B. Effect of nanoscale zero-valent iron and magnetite (Fe₃O₄) on the fate of metals during anaerobic digestion of sludge. *Water Res.* **2016**, *88*, 897–903. [[CrossRef](#)]
66. Gonzalez-Estrella, J.; Sierra-Alvarez, R.; Field, J. Toxicity assessment of inorganic nanoparticles to acetoclastic and hydrogenotrophic methanogenic activity in anaerobic granular sludge. *J. Hazard. Mater.* **2013**, *260*, 278–285. [[CrossRef](#)] [[PubMed](#)]
67. Rosicka, D.; Sembera, J. Assessment of influence of magnetic forces on aggregation of zero valent iron nanoparticles. *Nanoscale Res. Lett.* **2011**, *6*, 10–16. [[CrossRef](#)] [[PubMed](#)]
68. Tang, S.; Lo, I. Magnetic nanoparticles: Essential factors for sustainable environmental application. *Water Res.* **2013**, *47*, 2613–2632. [[CrossRef](#)] [[PubMed](#)]
69. Xu, P.; Zeng, G.; Huang, D.; Feng, C.; Hu, S.; Zhao, M.; Lai, C.; Wei, Z.; Huang, C.; Xie, G.; et al. Use of iron oxide nanomaterials in wastewater treatment: A review. *Sci. Total Environ.* **2012**, *424*, 1–10. [[CrossRef](#)] [[PubMed](#)]
70. Wu, W.; Wu, Z.; Yu, T.; Jiang, C.; Kim, W. Recent progress on magnetic iron oxide nanoparticles: Synthesis, surface functional strategies and biomedical application. *Sci. Technol. Adv. Mater.* **2015**, *16*, 1–43. [[CrossRef](#)] [[PubMed](#)]
71. Hutchins, D.; Downey, J. Effective separation of magnetite nanoparticles within an industrial scale pipeline reactor. *Sep. Sci. Technol.* **2019**, 1–8. [[CrossRef](#)]
72. Rui, M.; Ma, C.; Hao, Y.; Guo, J.; Rui, Y.; Tang, X.; Qi, Z.; Fan, X.; Zetian, Z.; Hou, T.; et al. Iron oxide nanoparticles as a potential iron fertilizer for peanut (*Arachis hypogaea*). *Front. Plant Sci.* **2016**, *7*, 815. [[CrossRef](#)]

73. Li, J.; Chang, P.; Huang, J.; Wang, Y.; Yuan, H.; Ren, H. Physiological effects of magnetic iron oxide nanoparticles towards watermelon. *J. Nanosci. Nanotechnol.* **2013**, *13*, 5561–5567. [[CrossRef](#)]
74. Boutchuen, A.; Zimmerman, D.; Aich, N.; Masud, A.; Arabshahi, A.; Palchoundhury, S. Increased plant growth with haematite nanoparticles fertilizer drop and determining nanoparticles uptake in plants using multimodal approach. *J. Nanomater.* **2019**, *2019*, 6890572. [[CrossRef](#)]
75. Elfeky, S.; Mohammed, M.; Khater, M.; Osman, Y.; Elsherbini, E. Effect of magnetite nano-fertilizer on growth and yield of *Ocimum basilicum* L. *Int. J. Indig. Med. Plants* **2013**, *46*, 1286–1293.
76. Plaksenkova, I.; Jermalonoka, M.; Bankovska, L.; Gavarane, I.; Gerbreders, V.; Sledevskis, E.; Snikeris, J.; Kokina, I. Effects of Fe₃O₄ nanoparticles stress on the growth and development of rocket *Eruca sativa*. *J. Nanomater.* **2019**, *2019*, 2678247. [[CrossRef](#)]
77. Abou El-Nasr, M.; El-Hennawy, H.; El-Kereamy, A.; Abou-El-Yazied, A.; Salah Eldin, T. Effect of magnetite nanoparticles (Fe₃O₄) as nutritive supplement on pear saplings. *Middle East J. Appl. Sci.* **2015**, *5*, 777–785.
78. Govea-Alcaide, E.; Masunaga, S.; De Souza, A.; Fajardo-Rosabal, L.; Effenberger, F.; Rossi, L.; Jardim, R. Tracking iron oxide nanoparticles in plant organs using magnetic measurements. *J. Nanoparticle Res.* **2016**, *18*, 305. [[CrossRef](#)]
79. Kanjana, D. Foliar study on effect of iron oxide nanoparticles as an alternate source of iron fertilizer to cotton. *Int. J. Chem. Stud.* **2019**, *7*, 4374–4379.



© 2020 by the authors. Licensee MDPI, Basel, Switzerland. This article is an open access article distributed under the terms and conditions of the Creative Commons Attribution (CC BY) license (<http://creativecommons.org/licenses/by/4.0/>).